Radboud Repository

Radboud University Nijmegen

PDF hosted at the Radboud Repository of the Radboud University Nijmegen

The following full text is an author's version which may differ from the publisher's version.

For additional information about this publication click this link.
http://hdl.handle.net/2066/75273

Mn clusterisation in $Ga_{1-x}Mn_xN$

D. Wang[1], X. Y. Zhang[1,*], J. Wang[2,3], S. Q. Wei[2], W. S. Yan[2], and D. W. Boukhvalov[4]

1   Department of Physics, Surface Physics Laboratory (National Key Laboratory), and Synchrotron Radiation Research Center, Fudan University, 220 Handan Road, Shanghai 200433, China

2   National Synchrotron Radiation Laboratory, University of Science and Technology of China, Hefei 230029, China

3   Shanghai Synchrotron Radiation Facility, Shanghai Institute of Applied Physics, Shanghai 201800, China

4   Institute for Molecules and Materials, Radboud University of Nijmegen,
NL-6525 ED Nijmegen, the Netherlands

Abstract

Local structure of Mn atoms in $Ga_{1-x}Mn_xN$ has been investigated by the Mn L_3 edge x-ray absorption spectrum (XAS) at total electron yield mode, which preferentially looks at atoms near the surface. A modeling defects configuration, the Mn_5 micro-clusters complexed with substitutional Mn_{Ga} and interstitial Mn_I is found for the higher Mn doping concentration. This new configuration is also confirmed by the total energy calculations.

Corresponding author, email address: xy-zhang@fudan.edu.cn

1. Introduction

The combination of electronic and magnetic properties in a single device opens many prospects for information technology [1]. To this end, the unique properties are found in the III-V diluted magnetic semiconductors (DMSs), in which the long range magnetic ordering between localized d-electrons of the magnetic impurities is thought to be mediated by an interaction with the itinerant valence electrons of the host semiconductor. Interests are further caused by the prediction of ferromagnetism at room temperature and even above in these materials [2-4]. Of the established DMSs, Mn-doped GaN films are predicted to have the higher Curie temperatures (T_C) above room temperature [5] and many efforts involving the controlled fabrication of these materials as well as to explore the characterization and their physical properties have been developed [6-8]. It has been suggested that the ferromagnetism (FM) in (Ga,Mn)N could arise from the formation of magnetic clusters [9]. Kane *et al.* reported that the room temperature ferromagnetic hysteresis was observed in epitaxial layers of $Ga_{1-x}Mn_xN$ with concentrations of up to $x = 0.015$ grown on c-sapphire substrates by metalorganic chemical vapour deposition, which might be due to either Mn-clustering on the atomic scale or the $Ga_{1-x}Mn_xN$ bulk alloy [10]. Zając *et al.* pointed out that different Mn_xN_y phases were responsible for ferromagnetic behavior of (Ga,Mn)N grown by the ammonothermal and chemical transport methods, and the Mn_xN_y phases could be either in the form of tiny clusters or they were of small volume. They thought that some of the Mn_xN_y phases were ferro/ferrimagnetic and thus provided (high-temperature) FM contribution to the total magnetization of (Ga,Mn)N samples [11]. However, K. Biswas *et al.* have prepared Mn-doped GaN nanocrystals under solvothermal conditions by keeping the temperature of the preparation around 350 °C.

All the nanocrystals show ferromagnetism at room temperature, and the secondary phases are unlikely to be formed under the preparative conditions employed [12]. Although a great deal of emphases has been placed on understanding the origin of the ferromagnetic behavior of GaMnN, it is still in debate. One of the reasons is the complexity and instability of DMS materials in the preparation processes, which are frequently affected by some untraceable factors. Recently, we studied the $3d$ electronic states of Mn dopants in $Ga_{1-x}Mn_xN$ by Mn L-edge X-ray absorption spectroscopy (XAS) measurements. We have shown that most of Mn atoms in $Ga_{1-x}Mn_xN$ are bivalent (Mn^{2+}) with the total spin $S=5/2$ and the p-d hybridization is strongly influenced by Mn doping concentrations. When x▯0.025▯the $Ga_{1-x}Mn_xN$ with stronger p-d hybridization is obtained [6]. In addition, our previous near edge x-ray absorption fine structure (NEXAFS) study in Mn K edge [13] shows that most Mn atoms locate at Ga substitutional sites, Mn_{Ga} at low Mn content and the Mn_4 clusters, being made of four Mn atoms, exist at the higher doping concentration. Edmonds et $al.$ [14] found that the interstitial Mn_I was relatively mobile and had a tendency to outdiffuse to the surface. It is not unreasonable to expect that the local structure of Mn atom should be different in bulk or near surface. The clusterisation of Mn in GaMnN might play an important role in magnetic properties and perhaps results in the non-reproducibility of good quality DMSs, especially when the grain sizes of GaMnN are small. The traditional method to study the different local structures in films in near surface layer is using the etching [14]. It would destruct the surface of the film and does not suit for thin films. In this paper, we investigate the Mn cluster structures in $Ga_{1-x}Mn_xN$ by using a nondestructive method based on the x-ray absorption studies at Mn L_3 edge.

2. Experimental

As we know, the x-ray penetration length is the reciprocal of the absorption coefficient. The x-ray penetration depths for the Mn K edge (6540 eV) and L edge (640 eV) incident energies are 3 μm and 70 nm, respectively. While the Mn L edge measurement is performed in total electron yield mode, only electrons that come from the sample within 50 Å of the surface layer, which is the electron escape depth, will be collected. Then, the escape depth of x-ray photons is about 1 μm. Therefore, the local structure of Mn in bulk can be studied by the K edge NEXAFS at its x-ray fluorescence mode [13], and the structure of atoms in the near surface layer can be monitored by using the L edge x-ray absorption in total electron yield mode.

Two cubic $Ga_{1-x}Mn_xN$ films about 0.3 μm thick with different Mn concentrations were prepared by the plasma-assisted molecular beam epitaxy (PA-MBE) on GaAs (001) substrates at the University of Nottingham [15]. The growth was performed under nitrogen-rich conditions and the substrate temperature was fixed at 140 °C. A GaAs buffer layer (about 0.15 μm thick) was first grown on the substrate to improve the quality of the $Ga_{1-x}Mn_xN$ layer. The concentrations of Mn were determined by the secondary ion mass spectrometry. Samples with x=2.5 at.% and 10 at.% were used in this work. The x-ray diffraction (XRD) measurements confirmed the structure of a zinc-blende type for both films.

The x-ray absorption spectra were recorded at room temperature in total electron yield mode at the beamline U18 of the National Synchrotron Radiation Laboratory (NSRL). The beamline covered an energy range from 100 to 1000 eV with a resolution of about 0.2 eV. The photon incident angle was set to be 50° to the surface normal. The Raman experiments were carried out in the backscattering geometry at room temperature using the 514.5 nm line of an Ar-ion laser as the excitation source.

3. Results and discussion

4

Figure 1 shows the experimental Mn L_3 edge XAS of $Ga_{1-x}Mn_xN$ thin films with two different Mn doping concentrations (x=2.5% and x=10%, respectively). Both spectra have been subtracted by the pre-edge background, and then normalized by the incident intensity I_0 and the maximum of the peak heights at the absorption edge. For the sample of x=2.5%, the L_3 edge exhibits one peak feature (labeled A) accompanied by a very small shoulder (labeled B) at the higher energy side. While for the higher Mn concentration (x=10%), the peak A becomes narrower and two additional peaks (labeled C and D) appear obviously in the high energy side of peak A. This profile is a specific characteristic of the highly localized d^5 ground state [16]. Y. Yonamoto *et al.* [17] and Y. Ishiwata *et al.* [18] thought that the large multiplet splitting feature resulted from the Mn oxide at surfaces due to highly sensitive of Mn L_3 edge spectra to the surface in total electron yield mode. Edmonds *et al.* [19] pointed out that the Mn oxide in the surface was less of an issue in the material (Ga,Mn)N than in (Ga,Mn)As. A shift of about 0.5 eV to higher energies should be observed in L_3 spectra after Mn oxidizing. However, no such an energy shift was observed in XAS spectra of our two samples. It seems that the large multiplet splitting feature in the 10% Mn doping concentration sample comes from Mn atoms but not from the surface oxide contamination.

As we know, various configurations of different Mn occupations associated with diverse kinds of adjacent defects will affect the local electronic structure of Mn atoms, which corresponds to different features in Mn L_3 edge XAS. For understanding the nature of Mn in zinc-blende $Ga_{1-x}Mn_xN$, the Mn L_3 edge XAS curves were calculated by FEFF 8.2 code [20]. Different representative models of the $Ga_{1-x}Mn_xN$ with various Mn occupation sites in GaN lattice are used for the XAS calculations. Several typical ones are shown in Fig. 2. They are substitutional Mn (Mn_{Ga}), interstitial Mn (Mn_I), Mn_4 micro-cluster (four congregated Mn_{Ga} neighbors) and Mn_5 micro-cluster (four neighbors

of Mn_{Ga} adding one Mn_I in the center). The XAS calculations of Mn_{Ga} or Mn_I with several possible defects as neighbors are also considered. The L_3 edge XAS calculations used the $Ga_{1-x}Mn_xN$ cluster with 123 atoms and carried out using initial ground-state potentials and a fully relaxed hole at the core level. The Dirac-Hara model of exchange potential with a 1.2 eV shift and an additional broadening of 0.1 eV is used for the L_3 edge XAS calculation. All calculations are done using the theoretical lattice constant (a= 4.46 Å).

Figures 3(a) and 3(b) show the calculated L_3 edge spectra using different Mn configurations as mentioned above. It can be seen that none of the calculated XAS spectra with one single type of Mn configuration can well fit the experimental results. Therefore, numbers of simulations based on various combinations of different Mn configurations are performed. The simulation curve of one substitutional Mn_{Ga} plus a Mn_{Ga} bound to an N vacancy nearby at a ratio of 1:1 reproduces most closely the experimental line shape of the sample at 2.5% Mn doping, as shown as curve *b* in Fig. 4, and the appearance of a shoulder B in curve *a* is mostly due to the N vacancy bound to the Mn atom nearby (cf. Fig. 3(b)). While for 10% Mn doped sample, the simulation is more complicated due to the narrower full width at half maximum (FWHM) as well as the appearance of a new peak D at higher energy side. The model, including the Mn_4 micro-cluster, Mn_I and $Mn_{Ga,}$ used in our previous NEXAFS study for Mn K edge [13], was first tested. Unfortunately, it could not give a satisfactory fitting. Then, as many as possible combined models were constructed. Some models that were more complicated than the one suitable for K edge XAS of GaMnN were used. The results show that a model made of Mn_5, Mn_{Ga}, and Mn_I is the most probable one. The simulation curve, a linear addition of calculated spectra of Mn_5, Mn_I, and Mn_{Ga} in ratio of 2:2:1 approximately, is well consistent with our experimental data, as shown as curve *d* in

Fig. 4. It surprised us that for two cases (K edge and L_3 edge), the only difference exists

between Mn$_4$ and Mn$_5$ micro-clusters.

To verify the possibility of forming Mn$_5$ micro-clusters, we carried out *ab initio*

calculations. For our calculations we used SIESTA pseudopotential code [21, 22],

which was before implemented to calculation of DMS [23]. In our calculation, we

studied the changes of formation energy per Mn atom for super-cell contained 32 atoms

of Ga and 32 atoms of N. The model concentration of Mn 15.6% is close to the

experimental one. Calculations of formation energies were performed by standard

formulas used in [23]. For verifying our method and technical parameters, we carried

out the LDA [24] calculation of pure GaN with full optimization of lattice parameters

and atomic positions. A small (less than 1%) compressing of lattice parameter from

experimental one was observed.

References [25, 26] suggest us for correct calculation of formation energy, which

is needed to find optimal magnetic configurations. For calculating the ground state of

Mn, we performed the calculation for antiferromagnetic (AFM) state of γ-Mn. For pair

of substitutional Mn in GaN, we found that the AFM configuration had a lower energy

than ferromagnetic one. For this configuration the formation energy was about 1.69 eV

per Mn, which was a little smaller than one for single substitutional Mn (1.77 eV) and

compressing of lattice parameter by about 1.5% from experimental one. Next, an

increase of Mn micro-clusters, which contained only substitutional Mn atoms, provided

a neglected decreasing of formation energy per Mn to 1.65 eV for Mn$_4$ micro-cluster

presented in Fig. 2(c). Next step in our modeling of Mn impurities in GaN was to study

the probability of forming micro-clusters, which contained substitutional and interstitial

atoms. The possibility of substitutional and interstitial dopants and their connection

with ferromagnetism in DMS thin films were discussed in Refs. [23, 27]. First we

calculated the formation energy per single interstitial Mn, which was 7.60 eV. However, the combination of substitutional and interstitial Mn provided a strong decreasing formation energy to 3.25 eV per Mn. We need to note that for this type of configuration, lower energy should correspond with the AFM configuration, which could be explained by the presence of a strong direct AFM Mn-Mn exchange as in pure γ-Mn. It is similar to the results reported recently in Ref. [28] about AFM coupling between substitutional and interstitial Mn. Then, an increase of the size of micro-clusters provided a decreasing of formation energy per Mn to 1.55 eV for Mn_5 micro-cluster, which contained four substitutional and one interstitial Mn atoms (see Fig. 2(d)). Compressing of lattice parameter for described Mn_5 micro-cluster is 0.4% from experimental one for pure GaN. Therefore, we can summarize that described micro-cluster is most favorable type of impurity in studied samples.

Based on our simulation above, it is concluded that the Mn atoms in the film is mostly Mn_{Ga} substitutions for 2.5% Mn doping concentration, and for 10% Mn doping concentration, in addition to substitutional Mn_{Ga} and interstitial Mn_I, more than 75% Mn atoms aggregate into Mn_5 micro-clusters. The formation of Mn_5 micro-clusters depends on the concentration of both Mn_{Ga} and Mn_I. The outdiffused Mn_I might accumulate at the surfaces of the $Ga_{1-x}Mn_xN$ film leading to not only the more possibility of the formation of Mn_5 micro-cluster, but also further decreasing the Mn_I in the bulk of the film. Consequently, the Mn atoms near the surface intend to be aggregated together in the form of Mn_5 micro-clusters, while Mn_4 micro-clusters in the bulk.

To obtain additional information about the incorporation of Mn ions into the GaN lattice, the Raman spectra of our samples are presented in Fig. 5. For comparing with our doping samples, the Raman spectra of the pure cubic GaN and the GaAs are also

given. The two peaks located at 550 cm^{-1} and 736 cm^{-1} are observed for both samples. They are the characteristic features of the cubic GaN (LO and TO vibrational modes) and also appear in the Raman spectrum of the pure cubic GaN, as shown in Fig. 5. The broader and asymmetric LO band means the lower electron concentration [29] due to the existence of defects and Mn_I in our films. Two peaks around 667 cm^{-1} and 586 cm^{-1} in the spectra of Mn doped samples are disorder-activated modes or local vibrational mode (LVM) of the GaN:Mn [30] and marked with "a" and "b" in the figure, respectively. These modes can be observed when long-range lattice ordering of the host lattice is lost. A relatively strong peak "a" is assigned to a LVM of GaN related to a N vacancy [31]. The peak "b" is assigned to the LVM of Mn occupying the Ga site. When the doping concentration is increased, the decreasing intensity of peak "b" means that the number of the substitutional Mn_{Ga} decreases. It is well consistent with above L_3 edge XAS studies.

4. Conclusion

In summary, we have shown that the Mn occupations in GaN are strongly influenced by the Mn doping concentrations and have different geometry configurations in near surface layer or in the bulk. Mn atoms near surfaces in $Ga_{1-x}Mn_xN$ can be directly probed by the Mn L_3 edge XAS. A new structural model of Mn_5 micro-clusters is proposed for the GaMnN surface layer, which explains well the L_3 edge XAS experimental results, and is also supported by our total energy calculations. The combined analysis of Mn L_3 edge and K edge XAS measurements is applied to identify the different clusterisation of Mn atoms near surface or in bulk and provides a useful method for understanding the cluster formation of Mn in GaMnN thin films.

Acknowledgements

References

[1] H. Ohno, Science **281** (1998) 951.

[2] A. Oiwa, Y. Mitsumori, R. Moriya, T. Slupinski, and H. Munekata, Phys. Rev. Lett. **88** (2002) 137202.

[3] Y. J. Zhao, T. Shishidou, and A. J. Freeman, Phys. Rev. Lett. **90** (2003) 047204.

[4] J. N. Gleason, M. E. Hjelmstad, V. D. Dasika, and R. S. Goldman, Appl. Phys. Lett. **86** (2005) 011911.

[5] T. Dietl, H. Ohno, F. Matsukura, J. Cibert, and D. Ferrand, Science **287** (2000) 1019.

[6] D. Wang, X. Y. Zhang, J. Wang and T. Koide, Solid State Communications **149**, (2009) 192.

[7] X. Luo and Richard M. Martin, Phys. Rev. **B 72** (2005) 035212.

[8] D. J. Keavney, S. H. Cheung, S. T. King, M. Weinert, and L. Li, Phys. Rev. Lett. **95** (2005) 257201.

[9] M. V Schilfgaarde and O. N. Mryasov, Phys. Rev. B **63** (2001) 233205.

[10] M. H. Kane, A. Asghar, C. R. Vestal, M. Strassburg, J. Senawiratne, Z. J. Zhang, N. Dietz, C. J. Summers and I. T. Ferguson, Semicond. Sci. Technol. **20** (2005) L5–L9.

[11] M. Zając, J. Gosk, E. Grzanka, M. Kamin´ska, A. Twardowski, B. Strojek, T. Szyszko, and S. Podsiadło, J. Appl. Phys., **93** (2003) 4715.

[12] K. Biswas, K. Sardar, and C. N. R. Rao, Appl. Phys. Lett. **89** (2006) 132503.

[13] S. Q. Wei, W. S. Yan, Z. H. Sun, Q. H. Liu, W. J. Zhong, X. Y. Zhang, H. Oyanagi and Z. Y. Wu, Appl. Phys. Lett. **89** (2006) 121901.

[14] K. W. Edmonds, P. Boguslawski, K. Y. Wang, R. P. Campion, S. N. Novikov, N. R. S. Farley, B. L. Gallagher, C. T. Foxon, M. Sawicki, T. Dietl, M. B. Nardelli, J. Bernholc, Phys. Rev. Lett. **92** (2004) 037201.

[15] S. V. Novikov, K. W. Edmonds, A. D. Giddings, K.Y. Wang, C. R. Staddon, R. P. Campion, B. L. Gallagher and C. T. Foxon, Semicond. Sci. Technol. **19** (2004) L13.

[16] G. van der Laan and I. W. Kirkman, J. Phys.: Condens. Matter **4** (1992) 4189.

[17] Y. Yonamoto, T. Yokoyama, K. Amemiya, D. Matsumura, and T. Ohta, Phys. Rev. B **63** (2001) 214406.

[18] Y. Ishiwata, M. Watanabe, R. Eguchi, T. Takeuchi, Y. Harada, A. Chainani, S. Shin, T. Hayashi, Y. Hashimoto, S. Katsumoto, and Y. Iye, Phys. Rev. B **65** (2002) 233201.

[19] K. W. Edmonds, N. R. S. Farley, T. K. Johal, R. P. Campoin, B. L. Gallagher, C. T. Foxon and G. van der Laan, J. Appl. Phys. **95** (2004) 7166.

[20] J. J. Rehr and R. C. Albers, Rev. Mod. Phys. **72** (2000) 621.

[21] E. Artacho, J. D. Gale, A. Garsia, J. Junquera, R. M. Martin, P. Orejon, D. Sanchez-Portal, J. M. Soler, SIESTA, Version 1.3 (2004).

[22] J. M. Soler, E. Artacho, J. D. Gale, A. Garsia, J. Junquera, P. Orejon, D. Sanchez-Portal, J. Phys.: Condens. Matter **14** (2002) 2745.

[23] G. S. Chang, E. Z. Kurmaev, D. W. Boukhvalov, L. D. Finkelstein, S. Colis, T. M. Pedersen, A. Moewes, and A. Dinia, Phys. Rev. B **75** (2007) 195215.

[24] J. P. Perdew and A. Zunger, Phys. Rev. B **23** (1981) 5048.

[25] D. W. Boukhvalov, Yu. N. Gornostyrev, M. I. Katsnelson, A. I. Lichtenstein, Phys. Rev. Lett. **99** (2007) 247205.

[26] A. Froideval, R. Iglesias, M. Samaras, S. Schuppler, P. Nagel, D. Grolimund, M. Victoria, W. Hoffelner, Phys. Rev. Lett. **99** (2007) 237201.

[27] G. S. Chang, E. Z. Kurmaev, D. W. Boukhvalov, L. D. Finkelstein, D. H. Kim, T.-W. Noh, A. Moewes and T. A. Callcott, J. Physics: Condensed Matter **18** (2006) 4243-4251.

[28] Q. H. Liu, Z. H Sun, W. S. Yan, W. J. Zhong, Z. Y. Pan, L. Y. Hao, and S. Q. Wei, Phys. Rev. B **76** (2007) 245210.

[29] T. Kozawa, T. Kachi, H. Kano, Y. Taga, and M. Hashimoto, J. Appl. Phys. **75** (1994) 1098.

[30] M. Zając, R. Doradziński, J. Gosk, J. Szczytko, M. Lefeld-Sosnowska, M. Kamińska, A. Twardowski, M. Palczewska, E. Grzanka and W. Gębicki, Appl. Phys. Lett. **78** (2001) 1276.

[31] W. Limmer, W. Ritter, R. Sauer, B. Mensching, C. Liu, and B. Rauschenbach, Appl. Phys. Lett. **72** (1998) 2589.
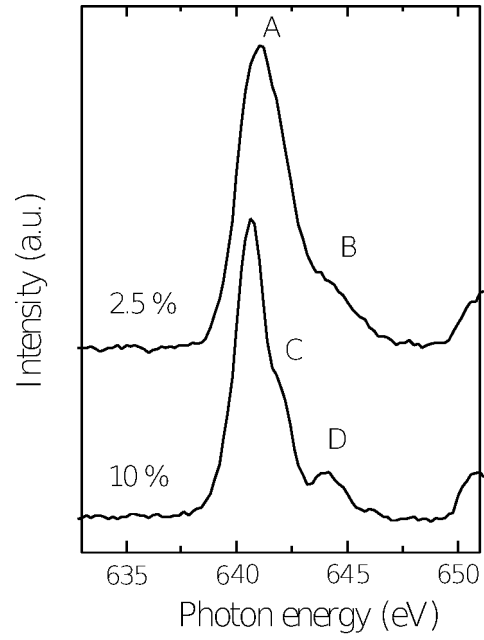
Figures

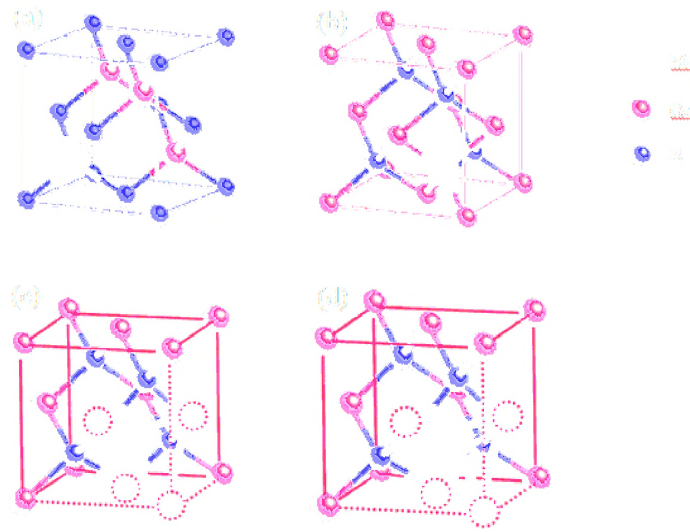Fig.1 Mn L_3 edge absorption spectra of $Ga_{1-x}Mn_xN$ thin films.

Fig.2 (Colour online) Model structures of various Mn occupation sites in GaN lattice: (a) substitutional Mn_{Ga}, (b) interstitial Mn_I, (c) Mn_4 micro-cluster and (d) Mn_5 micro-cluster. The empty circles with dotted-line border represent the locations in the zinc-blende structure.
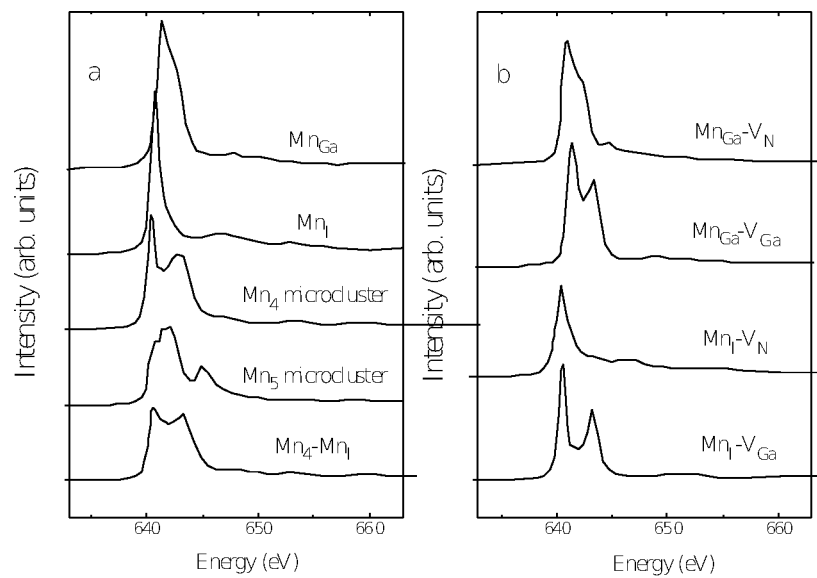
Fig.3 Calculated L_3 edge XAS spectra (a) for various Mn configurations in GaN lattice,

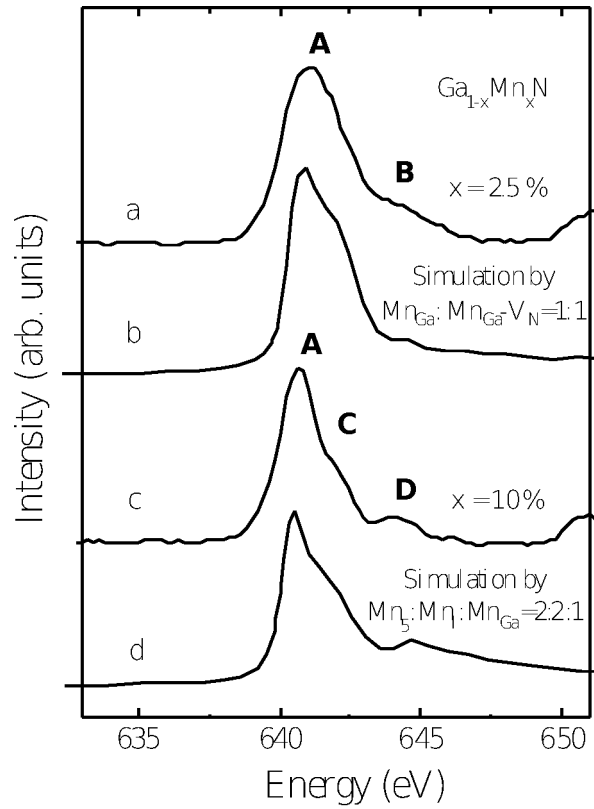and (b) with various related defects near the Mn atom in the film.

Fig.4 Comparison of the Mn L_3 edge XAS spectra from theoretical calculations and experimental spectra for $Ga_{1-x}Mn_xN$ with various Mn concentrations. Curves a and c are the experimental spectra for x=2.5% and 10%, respectively, and b and d, the simulation curves for both samples respectively.
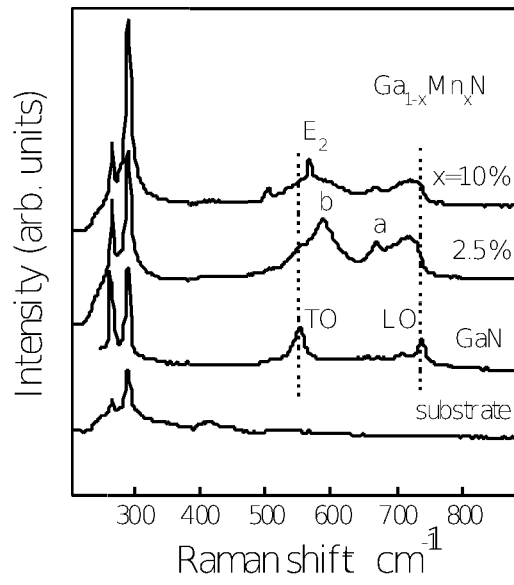
Fig.5 Raman spectra of $Ga_{1-x}Mn_xN$ films.